

An enriched 1D finite element for the buckling analysis of sandwich beam-columns

Kahina Sad Saoud¹ · Philippe Le Grogne¹

Received: 16 July 2015 / Accepted: 26 January 2016 / Published online: 18 February 2016
© Springer-Verlag Berlin Heidelberg 2016

Abstract Sandwich constructions have been widely used during the last few decades in various practical applications, especially thanks to the attractive compromise between a lightweight and high mechanical properties. Nevertheless, despite the advances achieved to date, buckling still remains a major failure mode for sandwich materials which often fatally leads to collapse. Recently, one of the authors derived closed-form analytical solutions for the buckling analysis of sandwich beam-columns under compression or pure bending. These solutions are based on a specific hybrid formulation where the faces are represented by Euler–Bernoulli beams and the core layer is described as a 2D continuous medium. When considering more complex loadings or non-trivial boundary conditions, closed-form solutions are no more available and one must resort to numerical models. Instead of using a 2D computationally expensive model, the present paper aims at developing an original enriched beam finite element. It is based on the previous analytical formulation, insofar as the skin layers are modeled by Timoshenko beams whereas the displacement fields in the core layer are described by means of hyperbolic functions, in accordance with the modal displacement fields obtained analytically. By using this 1D finite element, linearized buckling analyses are performed for various loading cases, whose results are confronted to either analytical or numerical reference solutions, for validation purposes.

Keywords Sandwich structures · Buckling/wrinkling · Compression/bending · Generalized eigenproblem · Numerical modeling

1 Introduction

Nowadays, numerous advanced industrial applications involve sandwich composites, taking advantage of their interesting combined mechanical, electrical, thermal and optical properties, among others. Such materials are commonly composed of two thin and stiff metallic or composite skins, separated by a thicker and much softer foam core. The resulting structure combines thus both an extreme lightweight due to the low density core material, and strong mechanical properties coming from the skins and their distance to the middle surface of the composite. In spite of all these benefits, sandwich materials suffer from some weaknesses, mostly inherent to their heterogeneous structure. Among them, the buckling phenomenon is known to be one of the major causes for the final collapse of such materials and therefore it has been the subject of numerous studies in the last few decades.

A significant amount of the existing numerical contributions on sandwich buckling rely on laminated composite displacement-based theories which are formulated on the basis of conventional assumptions for homogeneous beams/plates. In this respect, the most elementary bending models are based upon Euler–Bernoulli/Love–Kirchhoff hypotheses, stating that cross-sections initially perpendicular to the neutral axis/plane of the beam/plate remain straight and normal to the mid-axis/plane after deformation. As the transverse shear deformation effects are not included, these assumptions are no more valid when dealing with moderately thick structures. In order to overcome this shortcoming, first-order shear deformation theories (FSDT, also referred to

✉ Philippe Le Grogne
philippe.le.grogne@mines-douai.fr

¹ Mines Douai, Polymers and Composites Technology & Mechanical Engineering Department, 941 rue Charles Bourseul, CS 10838, 59508 Douai Cedex, France

as Timoshenko/Reissner-Mindlin theory for beams/plates) have emerged. They maintain that the deformed cross-sections remain plane, but not necessarily perpendicular to the deformed neutral axis/plane (see Timoshenko [1] and Reissner [2], for instance). The resulting shear strain distribution is uniform through the thickness (rather than parabolic in the case of a homogeneous structure) and thus, use is made of a shear correction factor to accurately assess the transverse shear force. The determination of this factor is usually not an easy task as it depends on many parameters such as the geometry, loading and boundary conditions (see Dong et al. [3] for further details). Therefore, as an alternative, higher-order shear deformation theories (HSDT) and refined shear deformation theories (RSDT) have been developed, which enable a more realistic description of the shear strain distribution (without any correction), thanks to the introduction of non-linear terms in the displacement fields. The enrichment functions (for the longitudinal/in-plane displacements) may range from polynomials (among many other authors, Ambartsumian [4] and Reddy [5] illustrated the well-known case of third-order kinematics) and trigonometric functions (for instance, ordinary and hyperbolic sine/cosine functions were respectively used in Touratier [6] and Soldatos [7]) to exponential functions (see, for example, Sayyad [8]). Besides, it would be worth-mentioning that the transverse deflection is in almost all cases assumed to be constant along the thickness direction.

The main benefit of such approaches lies in their greater efficiency when compared to onerous 2D/3D models. Dealing with laminated composites, one can distinguish between two main approaches, namely the equivalent single-layer (ESL) and layer-wise (LW) theories, according to whether the kinematic fields are described in a global or discrete way. The main differences between these two approaches are schematically represented in Fig. 1, in the case of a sandwich structure.

In ESL theories, the displacement field is assumed to be represented by a unique expression across the whole

thickness of the composite structure. This may lead to acceptable global stress distributions but completely inappropriate results regarding the interlaminar stresses, and increasing the order of the displacement field is not supposed to fix the problem [10]. For a detailed literature review on the use of the existing ESL theories in the general case of laminated composites, the interested reader may refer to Reddy [11] and Carrera [12], for instance.

In contrast, LW theories rely on piecewise displacement fields, which offer a more realistic representation of the composite through-thickness kinematics. Discrete LW theories assume independent displacement fields within each layer, thus making the number of kinematic variables dependent on the number of layers. The displacement continuity conditions at the interfaces between adjacent layers enable then the total number of degrees of freedom to be reduced [13, 14]. In order to minimize the computational cost of the discrete LW class models, one can resort to the well-known zig-zag theory, initially introduced by Di Sciuva [15]. In zig-zag models, the in-plane displacements are first defined in a global way (generally using a first-order representation) and then supplemented by piecewise zig-zag functions which ensure the continuity of displacements but also transverse stresses at each interface between successive layers (an overview on zig-zag and refined zig-zag models is available in Tessler et al. [16]). Advanced solutions such as those based on Carrera's unified formulation (CUF) or generalized unified formulation (GUF) have emerged recently. Further details on these methods may be found for instance in Carrera [17] and Demasi [9], and benchmark analyses of many theories and models are gathered in the review articles by Ghugal and Shimpi [18], Zhen and Wanji [19] and Hu et al. [20].

The above-mentioned theories have been so far widely applied to investigate the behavior of sandwich structures, which can be viewed as special laminated composites. However, dealing with classical sandwich structures, with typically uniform thick and soft core materials compared to

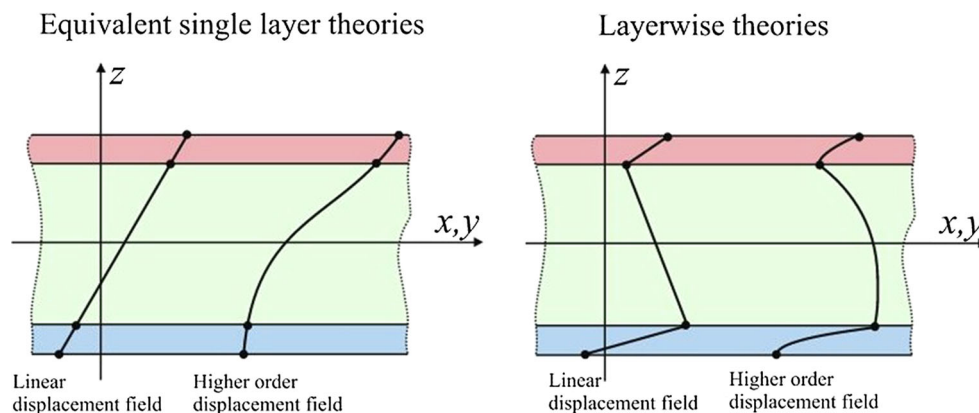


Fig. 1 Illustration of a displacement field in a sandwich beam in the context of ESL and LW theories [9]

the skins, the above model classes are still not appropriate tools to accurately describe the complex behavior of the core layer, especially when the faces are intended to wrinkle.

Phan et al. [21] have shown that considering linear axial strain distribution in the core layer may lead to erroneous results, even for moderately thick cores. A few years earlier, Hu et al. [22] built on a specific formulation so as to develop a 1D beam-like finite element model, wherein the skins are represented by an Euler–Bernoulli beam model while the transverse and axial displacements in the core layer are second- and third-order polynomial functions of the thickness coordinate, respectively. Despite these non-linear displacement fields used in the kinematic description, the critical buckling loads obtained with their model differ from 2D numerical simulation results as soon as wrinkle modes are concerned.

Therefore, the present study aims at developing a new specific 1D finite element model devoted to the analysis of sandwich beams. Such a 1D model is meant to be an efficient numerical tool compared to a classical 2D finite element model, where both the skin and core layers are represented as 2D continuous media and discretized using solid elements. Moreover, in the interest of accuracy, a particular emphasis is given to the through-thickness kinematics. While the skins are typically modeled by Timoshenko beams, the displacement fields in the core layer are not chosen arbitrarily but defined in accordance with analytical solutions which were derived by the authors in the context of buckling analyses of sandwich beam-columns and plates under various loadings, without presupposing any kinematic assumption [23,24].

The original finite element formulation is implemented in a home-made program whose main objective is to analyze

the global and local buckling behavior of sandwich beam-columns. For this purpose, linearized buckling analyses are performed within a total Lagrangian framework. Numerical results are compared with the analytical solutions from Douville and Le Grogneq [23] and reference results from 2D finite element computations performed for validation purposes.

2 Theoretical formulation

2.1 Problem statement

This study focuses on classical symmetric sandwich beam-columns (with identical skins). As in Douville and Le Grogneq [23], the sandwich structure is of length L , thicknesses $2h_s$ and $2h_c$ (for the skin and core layers, respectively) and unit depth. Both skin and core materials are assumed to be homogeneous and isotropic with a linear elastic constitutive law (use is made of the Young’s moduli E and the Poisson’s ratios ν but also of the Lamé constants Λ and μ where $\Lambda = \frac{E\nu}{(1+\nu)(1-2\nu)}$ and $\mu = \frac{E}{2(1+\nu)}$ stands for the shear modulus). The final objective is to define a ‘sandwich beam’ model in order to investigate the global but also local behavior of such a composite structure in an efficient way. The buckling response of the sandwich structure is of special interest, since it particularly involves multi-scale phenomena. Among the loading conditions giving rise to global or local instabilities (see Fig. 2), the cases of compression and pure bending have already been solved analytically in Douville and Le Grogneq [23]. In particular, the analytical modal deformation shapes of the core layer, obtained without the use of any kinematic assumption, have shown to be very similar for both loading

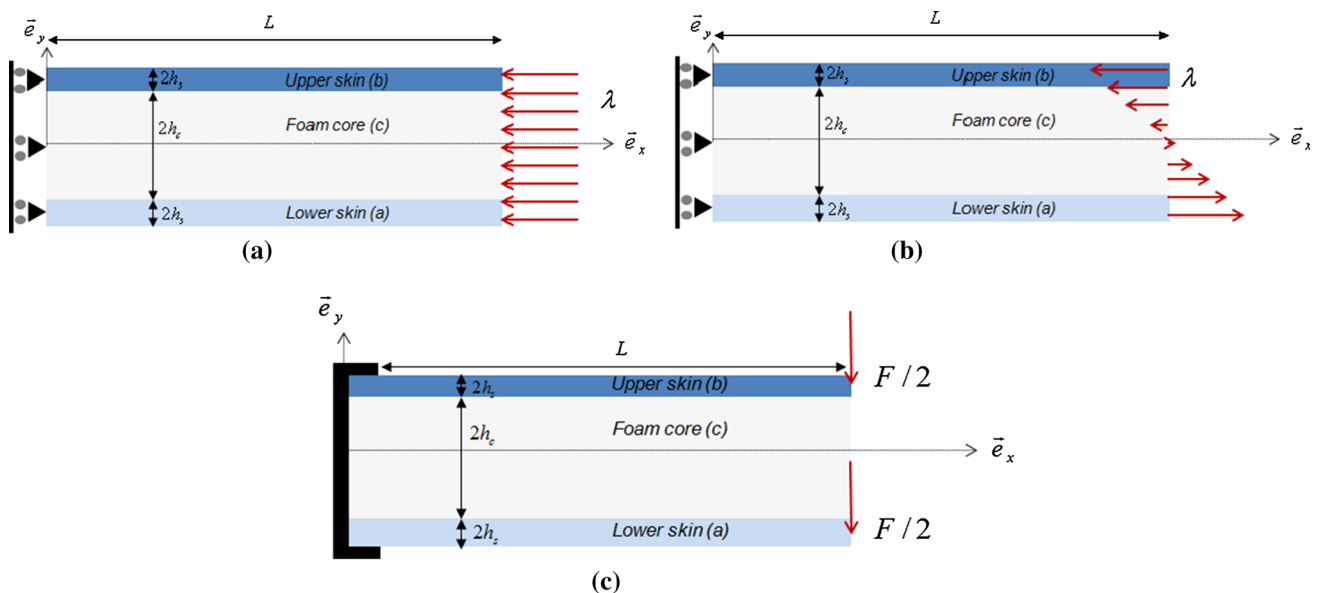


Fig. 2 Two-dimensional representation of a sandwich beam-column under various loading conditions. **a** sandwich column under compression, **b** sandwich beam under pure bending, **c** sandwich beam under simple bending

conditions, and they will thus serve as a basis for the definition of the 1D enriched numerical model.

2.2 General overview of the prior analytical results

In Douville and Le Grogneec [23], the facings are assumed to behave like Euler–Bernoulli beams, whereas the foam core is modeled by a 2D continuous solid satisfying the plane stress hypothesis. The left and right end sections of the sandwich column are respectively subjected to zero and non-zero displacement boundary conditions in the longitudinal direction (as depicted in Figs. 2a, b, in the compression and pure bending cases, respectively), what leads to buckling. The critical displacements λ_{cr} and the associated bifurcation modes are obtained by solving the so-called bifurcation equation in a 3D framework, following a total Lagrangian formulation.

Introducing the proper kinematics in each layer and with the help of a few simplifying assumptions, the bifurcation equation turns into a set of partial differential equations and associated natural boundary conditions, after integration by parts. Thanks to the additional displacement continuity and boundary conditions, the resulting system can be solved for the two considered loading cases (see Douville and Le Grogneec [23] for more details on the derivation of the governing equations).

In both cases, the following expressions can be used for the skin components of the bifurcation mode by extrapolating the classical buckling modes of a single beam with the same boundary conditions:

$$\begin{cases} \mathcal{U}_a = \alpha \sin \frac{n\pi X}{L} \\ \mathcal{U}_b = \beta \sin \frac{n\pi X}{L} \\ \mathcal{V}_a = \delta \cos \frac{n\pi X}{L} \\ \mathcal{V}_b = \cos \frac{n\pi X}{L} \end{cases} \quad (1)$$

where \mathcal{U}_i and \mathcal{V}_i (with $i = a$ or b depending on the considered skin) represent the longitudinal and transverse displacements of the neutral axis, according to the Euler–Bernoulli kinematics, n is an arbitrary half-wave number and α , β , δ are unknown amplitudes.

On one hand, dealing with the axial compression case, the same unit amplitude is retained for the transverse deflection of both faces, due to the symmetry of the problem. However, two cases should be considered, depending on the relative sign of the two fields \mathcal{V}_a and \mathcal{V}_b . The bifurcation mode of the sandwich column may thus be antisymmetric ($\delta = 1$, $\mathcal{V}_a = \mathcal{V}_b$) or symmetric ($\delta = -1$, $\mathcal{V}_a = -\mathcal{V}_b$).

Concerning the modal displacement field in the foam core, a separation of variables is performed and the following forms are presupposed, according to Eq. (1):

$$\begin{cases} \mathcal{U}_c = \zeta(Y) \sin \frac{n\pi X}{L} \\ \mathcal{V}_c = \xi(Y) \cos \frac{n\pi X}{L} \end{cases} \quad (2)$$

Solving first the two partial differential equations related to the core region, one gets the following expressions for functions ζ and ξ in the case of an antisymmetric mode:

$$\begin{cases} \zeta(Y) = k_1 \sinh \frac{n\pi Y}{L} + k_2 Y \cosh \frac{n\pi Y}{L} \\ \xi(Y) = k_3 \cosh \frac{n\pi Y}{L} + k_4 Y \sinh \frac{n\pi Y}{L} \end{cases} \quad (3)$$

where k_1 , k_2 , k_3 and k_4 are constants which depend on α and β . These two amplitudes are easily determined by solving two of the remaining partial differential equations derived in the upper and lower skins and turn out to be opposite from each other. The last two equations can be finally solved separately and both lead to the same closed-form expression for the critical displacement (see Eq. (33) in Appendix A). The same procedure is used in the case of a symmetric mode and gives rise to somewhat different expressions, in which the roles of functions ζ and ξ are reversed (see Eq. (34) for the new expression of the critical displacement).

On the other hand, in the pure bending case, the lower skin undergoes tensile stresses and is not subjected to any instability phenomenon. Nevertheless, it also deforms in a sine wave pattern, induced by the sinusoidal buckled shape of the compressed upper skin, but with a smaller amplitude of deflection ($\delta < 1$) and also a different amplitude of longitudinal displacement. The displacement field in the core layer is, however, split similarly as in Eq. (2). The solution procedure is finally analogous to the one described above. The only difference occurs when solving the last two partial differential equations, which are no more redundant, due to the different signs of the pre-critical stresses in the two facings. Here, these two equations allow one to derive both expressions of the critical displacement λ_{cr} and the amplitude δ (these closed-form expressions are not reported herein as they are quite bulky). What is important is that the same combinations of hyperbolic sine and cosine functions are established again for ζ and ξ .

In the sequel, the closed-form expressions obtained for the modal displacements in the core layer (functions ζ and ξ) will inspire the kinematics of the 1D enriched formulation to be defined. Besides, the previous analytical critical values will serve as reference solutions for future validation of the finite element model developed in this study.

2.3 1D formulation

The 'sandwich beam' model further developed relies on specific kinematic assumptions for each layer (skins and core) so as to properly describe the through-thickness distribution of strains and stresses, including when local instabilities occur in the sandwich.

2.3.1 Skin layers

For convenience purposes, the skin layers are represented by a Timoshenko beam model accounting for transverse shear effects, what allows one to deal with all kinds of sandwich beam-columns, including short ones.

Let $(\mathbf{e}_X, \mathbf{e}_Y, \mathbf{e}_Z)$ be a fixed orthonormal basis, where \mathbf{e}_X is the neutral axis of the beam in hand and \mathbf{e}_Y represents the thickness direction. The displacement field in each face may thus be expressed as follows, in the associated coordinate system:

$$\mathbf{U}(X, Y) = \begin{pmatrix} U(X) - Y\theta(X) \\ V(X) \\ 0 \end{pmatrix} \tag{4}$$

where $U(X)$ and $V(X)$ are respectively the longitudinal and transverse displacements of the centroid axis of the beam, and $\theta(X)$ represents the rotation of the cross-section about the \mathbf{e}_Z axis, in accordance with Timoshenko kinematics.

The Green-Lagrange strain tensor writes then:

$$\mathbf{E} = \frac{1}{2}(\nabla\mathbf{U} + \nabla^T\mathbf{U} + \nabla^T\mathbf{U} \cdot \nabla\mathbf{U}) \tag{5}$$

where the displacement gradient tensor $\nabla\mathbf{U}$ takes the following form in the orthonormal basis $(\mathbf{e}_X, \mathbf{e}_Y, \mathbf{e}_Z)$:

$$\nabla\mathbf{U} = \begin{bmatrix} U_{,x} - Y\theta_{,x} & -\theta & 0 \\ V_{,x} & 0 & 0 \\ 0 & 0 & 0 \end{bmatrix} \tag{6}$$

Hence, neglecting higher-order terms, the remaining non-zero strain-displacement relations may be expressed as follows:

$$\begin{cases} E_{XX} = U_{,x} + \frac{1}{2}V_{,x}^2 \\ 2E_{XY} = V_{,x} - (1 + U_{,x})\theta \end{cases} \tag{7}$$

In the general case of an isotropic linear elastic material, the Green-Lagrange strain tensor is related to the second Piola-Kirchhoff stress tensor by the Saint-Venant-Kirchhoff law:

$$\boldsymbol{\Sigma} = \mathbf{D} : \mathbf{E} = \Lambda \text{tr}(\mathbf{E})\mathbf{I} + 2\mu\mathbf{E} \tag{8}$$

where \mathbf{I} stands for the second-order unit tensor. Here, only the following non-zero stress components will be involved in the subsequent developments:

$$\begin{cases} \Sigma_{XX} = E_s E_{XX} \\ \Sigma_{XY} = 2\mu_s E_{XY} \end{cases} \tag{9}$$

2.3.2 Core layer

According to the preceding analytical developments, special kinematic expressions are introduced so as to describe the actual behavior of the homogeneous foam core.

The enriched displacement field in the core layer is written as follows:

$$\mathbf{U}^c(X, Y) = \begin{pmatrix} U_0^c(X) + U_1^c(X) \sinh(\frac{\pi}{L}Y) + F(X, Y) \\ V_0^c(X) \cosh(\frac{\pi}{L}Y) + V_1^c(X)Y + G(X, Y) \end{pmatrix} \tag{10}$$

where Y stands for the thickness coordinate relative to the mid-axis of the core layer.

The enrichment functions F and G are devoted to the description of the local effects that are likely to happen in the core layer. They are thus defined, in accordance with the analytical expressions of the buckling modes, as the following combinations of hyperbolic sine and cosine functions:

$$\begin{cases} F(X, Y) = \phi_1(X) \cosh(\alpha Y) + \phi_2(X) \sinh(\alpha Y) \\ \quad + \phi_3(X)Y \cosh(\alpha Y) + \phi_4(X)Y \sinh(\alpha Y) \\ G(X, Y) = \phi_5(X) \cosh(\alpha Y) + \phi_6(X) \sinh(\alpha Y) \\ \quad + \phi_7(X)Y \cosh(\alpha Y) + \phi_8(X)Y \sinh(\alpha Y) \end{cases} \tag{11}$$

A unique value of parameter α (replacing $\frac{n\pi}{L}$ in the analytical expressions) will be retained in the sequel, as it only depends on the wavelength $\frac{L}{n}$ which has proved to change practically very little when varying the geometric and material properties, as far as the first local mode is concerned. The amplitudes $\phi_2(X)$, $\phi_3(X)$, $\phi_5(X)$ and $\phi_8(X)$ are connected to the shape functions associated to the antisymmetric modes and, conversely, $\phi_1(X)$, $\phi_4(X)$, $\phi_6(X)$ and $\phi_7(X)$ are related to symmetric modes. In order to also represent the contribution of the global mode, similar functions are used (with amplitudes $U_1^c(X)$ and $V_0^c(X)$) where α is replaced by $\frac{\pi}{L}$ (considering $n = 1$ in the analytical expressions). The functions $Y \cosh(\frac{\pi Y}{L})$ and $Y \sinh(\frac{\pi Y}{L})$ are not introduced here as they would give rise to singularities due to redundancy. Indeed, since $Y \ll L$, these functions are far too close to the previous ones, $\sinh(\frac{\pi Y}{L})$ and $\cosh(\frac{\pi Y}{L})$, respectively. It is worth mentioning that the two functions $\sinh(\frac{\pi Y}{L})$ and $\cosh(\frac{\pi Y}{L})$ are almost linear and constant, respectively, in the range of the considered values, so that they can reproduce properly the deformation state of the core layer under pure or simple bending. Lastly, a constant component $U_0^c(X)$ and a linear one $V_1^c(X)Y$ have been added in the expressions of the longitudinal and transverse displacements, respectively, so as to reproduce also the deformation state under pure compression.

Then, the in-plane terms of the Green-Lagrange strain tensor may be expressed as follows:

$$\begin{cases} E_{XX}^c = \mathcal{H}_{XX}^c + \frac{1}{2} ((\mathcal{H}_{XX}^c)^2 + (\mathcal{H}_{YX}^c)^2) \\ E_{YY}^c = \mathcal{H}_{YY}^c + \frac{1}{2} ((\mathcal{H}_{YY}^c)^2 + (\mathcal{H}_{XY}^c)^2) \\ 2E_{XY}^c = \mathcal{H}_{XY}^c + \mathcal{H}_{YX}^c + \mathcal{H}_{XX}^c \mathcal{H}_{XY}^c + \mathcal{H}_{YY}^c \mathcal{H}_{YX}^c \end{cases} \quad (12)$$

where the components of the displacement gradient tensor \mathcal{H}^c are given in Eq. (35) (see Appendix B).

The facings are supposed to be perfectly bound to the core layer and ad hoc relationships are thus added so as to account for the continuity of the displacements at the top and bottom interfaces, bringing the total number of kinematic unknowns to 14:

• at the upper skin/core interface:

$$\begin{aligned} \mathbf{U}^b(X, -h_s) &= \mathbf{U}^c(X, h_c) \\ \implies \begin{cases} U^b + h_s \theta^b = U_0^c + U_1^c \sinh(\frac{\pi}{L} h_c) \\ \quad + \phi_1 \cosh(\alpha h_c) + \phi_2 \sinh(\alpha h_c) \\ \quad + \phi_3 h_c \cosh(\alpha h_c) + \phi_4 h_c \sinh(\alpha h_c) \\ V^b = V_0^c \cosh(\frac{\pi}{L} h_c) + V_1^c h_c \\ \quad + \phi_5 \cosh(\alpha h_c) + \phi_6 \sinh(\alpha h_c) \\ \quad + \phi_7 h_c \cosh(\alpha h_c) + \phi_8 h_c \sinh(\alpha h_c) \end{cases} \end{aligned} \quad (13)$$

• at the lower skin/core interface:

$$\begin{aligned} \mathbf{U}^a(X, h_s) &= \mathbf{U}^c(X, -h_c) \\ \implies \begin{cases} U^a - h_s \theta^a = U_0^c - U_1^c \sinh(\frac{\pi}{L} h_c) \\ \quad + \phi_1 \cosh(\alpha h_c) - \phi_2 \sinh(\alpha h_c) \\ \quad - \phi_3 h_c \cosh(\alpha h_c) + \phi_4 h_c \sinh(\alpha h_c) \\ V^a = V_0^c \cosh(\frac{\pi}{L} h_c) - V_1^c h_c \\ \quad + \phi_5 \cosh(\alpha h_c) - \phi_6 \sinh(\alpha h_c) \\ \quad - \phi_7 h_c \cosh(\alpha h_c) + \phi_8 h_c \sinh(\alpha h_c) \end{cases} \end{aligned} \quad (14)$$

where the superscripts \bullet^a and \bullet^b designate the bottom and top skin layers, respectively.

Taking into consideration the aforementioned displacement continuity constraints, one can rewrite ϕ_1, ϕ_2, ϕ_5 and ϕ_6 in terms of the remaining unknowns as follows:

$$\begin{aligned} \phi_1 &= \frac{1}{\cosh(\alpha h_c)} \left(\frac{1}{2} (U^b + U^a) + \frac{h_s}{2} (\theta^b - \theta^a) \right. \\ &\quad \left. - U_0^c - \phi_4 h_c \sinh(\alpha h_c) \right) \\ \phi_2 &= \frac{1}{\sinh(\alpha h_c)} \left(\frac{1}{2} (U^b - U^a) + \frac{h_s}{2} (\theta^b + \theta^a) \right. \\ &\quad \left. - U_1^c \sinh(\frac{\pi}{L} h_c) - \phi_3 h_c \cosh(\alpha h_c) \right) \end{aligned}$$

$$\begin{aligned} \phi_5 &= \frac{1}{\cosh(\alpha h_c)} \left(\frac{1}{2} (V^b + V^a) - V_0^c \cosh(\frac{\pi}{L} h_c) \right. \\ &\quad \left. - \phi_8 h_c \sinh(\alpha h_c) \right) \\ \phi_6 &= \frac{1}{\sinh(\alpha h_c)} \left(\frac{1}{2} (V^b - V^a) - V_1^c h_c - \phi_7 h_c \cosh(\alpha h_c) \right) \end{aligned} \quad (15)$$

Thereafter, the plane stress hypothesis is adopted so that the stress-strain constitutive law in the foam core writes:

$$\begin{bmatrix} \Sigma_{XX}^c \\ \Sigma_{YY}^c \\ \Sigma_{XY}^c \end{bmatrix} = \begin{bmatrix} \Lambda_c^* + 2\mu_c & \Lambda_c^* & 0 \\ \Lambda_c^* & \Lambda_c^* + 2\mu_c & 0 \\ 0 & 0 & \mu_c \end{bmatrix} \begin{bmatrix} E_{XX}^c \\ E_{YY}^c \\ 2E_{XY}^c \end{bmatrix} \quad (16)$$

where $\Lambda_c^* = \frac{2\Lambda_c \mu_c}{\Lambda_c + 2\mu_c}$.

3 Numerical implementation

3.1 Finite element model

The governing equations of the problem are derived from the principle of virtual work within a total Lagrangian framework. The following relation holds for any kinematically admissible displacement variation $\delta \mathbf{U}$:

$$\delta \mathcal{W}_{int}(\delta \mathbf{U}) + \delta \mathcal{W}_{ext}(\delta \mathbf{U}) = 0 \quad (17)$$

On one hand, the virtual internal work $\delta \mathcal{W}_{int}$ takes the following form:

$$\begin{aligned} \delta \mathcal{W}_{int} &= - \sum_{i=a,b,c} \int_{\Omega_i} \boldsymbol{\Sigma}^i : \delta \mathbf{E}^i dV_i \\ &= - \int_0^L \left(\int_{-h_s}^{h_s} (\Sigma_{XX}^a \delta E_{XX}^a + 2\Sigma_{XY}^a \delta E_{XY}^a) dY \right. \\ &\quad \left. + \int_{-h_c}^{h_c} (\Sigma_{XX}^c \delta E_{XX}^c + \Sigma_{YY}^c \delta E_{YY}^c + 2\Sigma_{XY}^c \delta E_{XY}^c) dY \right. \\ &\quad \left. + \int_{-h_s}^{h_s} (\Sigma_{XX}^b \delta E_{XX}^b + 2\Sigma_{XY}^b \delta E_{XY}^b) dY \right) dX \end{aligned} \quad (18)$$

Let us introduce the generalized strain vector $\boldsymbol{\gamma} = \langle E_{XX}^a, 2E_{XY}^a, E_{XX}^c, E_{YY}^c, 2E_{XY}^c, E_{XX}^b, 2E_{XY}^b \rangle^T$ and stress vector $\mathbf{s} = \langle \Sigma_{XX}^a, \Sigma_{XY}^a, \Sigma_{XX}^c, \Sigma_{YY}^c, \Sigma_{XY}^c, \Sigma_{XX}^b, \Sigma_{XY}^b \rangle^T$.

Then, one may define the following vector of generalized displacements:

$$\mathbf{q} = \left(U^b \ U^a \ U_{,X}^b \ U_{,X}^a \ V^b \ V^a \ V_{,X}^b \ V_{,X}^a \ \theta^b \ \theta^a \ \theta_{,X}^b \ \theta_{,X}^a \ U_1^c \ U_{1,X}^c \ V_0^c \ V_{0,X}^c \ \phi_3 \ \phi_4 \ \phi_7 \ \phi_8 \ \phi_{3,X} \ \phi_{4,X} \ \phi_{7,X} \ \phi_{8,X} \ U_0^c \ U_{0,X}^c \ V_1^c \ V_{1,X}^c \right)^T \tag{19}$$

where the functions $\phi_1, \phi_2, \phi_5, \phi_6$ and their derivatives have been discarded, since they are related to the other variables through the continuity conditions (see Eq. (36) in Appendix B for the corresponding expressions of the derivatives).

In order to establish more convenient expressions, vector $\boldsymbol{\gamma}$ (along with \mathbf{s}) may be split into a linear part and a quadratic one with respect to vector \mathbf{q} :

$$\begin{cases} \boldsymbol{\gamma} = \left(\mathbf{H} + \frac{1}{2}\mathbf{A}(\mathbf{q}) \right) \mathbf{q} \\ \mathbf{s} = \mathcal{L} \left(\mathbf{H} + \frac{1}{2}\mathbf{A}(\mathbf{q}) \right) \mathbf{q} \end{cases} \tag{20}$$

where $\mathbf{H}, \mathbf{A} \in \mathbb{R}^{7 \times 28}$, while the constitutive matrix $\mathcal{L} \in \mathbb{R}^{7 \times 7}$ (the corresponding formulae are given in Appendix C except from the components of matrix \mathbf{A} which are not reported due to their bulky size).

Hence, Eq. (18) takes the following vector form:

$$\begin{aligned} \delta \mathcal{W}_{int} &= - \int_0^L \left(\int_{-h_k}^{h_k} \delta \boldsymbol{\gamma}^T \mathbf{s} \, dY \right) dX \\ &= - \int_0^L \left(\int_{-h_k}^{h_k} \delta \mathbf{q}^T (\mathbf{H}^T + \mathbf{A}^T(\mathbf{q})) \mathcal{L} \left(\mathbf{H} + \frac{1}{2}\mathbf{A}(\mathbf{q}) \right) \mathbf{q} \, dY \right) dX \end{aligned} \tag{21}$$

in which the index $k = s$ or c , depending on the region in which the through-thickness integration is performed.

On the other hand, the only applied forces that will be considered in the sequel are localized at the two ends of the sandwich beam-column. The external virtual work $\delta \mathcal{W}_{ext}$ can thus be written as follows:

$$\delta \mathcal{W}_{ext} = \delta \mathbf{q}^T(0) \boldsymbol{\Phi}_0 + \delta \mathbf{q}^T(L) \boldsymbol{\Phi}_L \tag{22}$$

In Eq. (22), $\boldsymbol{\Phi}_0$ and $\boldsymbol{\Phi}_L$ represent vectors of generalized forces. Since in practice only the facings will be involved with the applied forces, the last 16 components of $\boldsymbol{\Phi}_0$ and $\boldsymbol{\Phi}_L$, associated to the core generalized displacements, will always be zero.

It should be mentioned that the integration of Eq. (21) with respect to the Y -coordinate is performed analytically through the thickness of the skins, while a numerical integration using Gaussian quadratures is carried out through the core thickness as it involves more complex hyperbolic functions. The resulting shear quantities in the skin layers ($\int_{-h_s}^{h_s} 2\delta E_{XY}^a \Sigma_{XY}^a \, dY$ and $\int_{-h_s}^{h_s} 2\delta E_{XY}^b \Sigma_{XY}^b \, dY$) are further

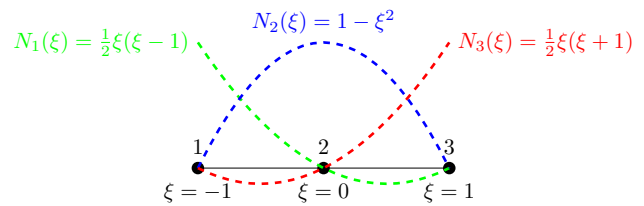


Fig. 3 Graphic representation of the interpolation functions of the 3-node reference 1D element

multiplied by a correction factor of $\frac{5}{6}$, as for homogeneous beams according to the Timoshenko beam theory.

The problem is now discretized using 3-node isoparametric elements with quadratic shape functions (see Fig. 3).

In view of the kinematic assumptions and continuity conditions, there remain 14 fundamental unknowns which can be brought together in a unique vector $\mathbf{d}(X) = \left(U^b(X) \ U^a(X) \ V^b(X) \ V^a(X) \ \theta^b(X) \ \theta^a(X) \ U_1^c(X) \ V_0^c(X) \ \phi_3(X) \ \phi_4(X) \ \phi_7(X) \ \phi_8(X) \ U_0^c(X) \ V_1^c(X) \right)^T$.

Within a given finite element e , all the components of vector \mathbf{d} are interpolated in the same way, introducing the elementary nodal displacement vector \mathbf{d}^e composed of the 42 degrees of freedom of the given element and the associated interpolation matrix \mathbf{N} :

$$\mathbf{d} = \mathbf{N} \mathbf{d}^e \tag{23}$$

with $\mathbf{d}^e = \left\langle \mathbf{d}_1^{eT} \ \mathbf{d}_2^{eT} \ \mathbf{d}_3^{eT} \right\rangle^T$, where $\mathbf{d}_i^e \triangleq \mathbf{d}(X_i) = \left\langle U^b \ U^a \ V^b \ V^a \ \theta^b \ \theta^a \ U_1^c \ V_0^c \ \phi_3 \ \phi_4 \ \phi_7 \ \phi_8 \ U_0^c \ V_1^c \right\rangle_i^T$ contains the 14 degrees of freedom of the i -th node of element e .

Finally, the generalized displacement vector \mathbf{q} may be expressed in terms of \mathbf{d} (by means of a transformation matrix \mathbf{T} including differential operators) and subsequently in terms of \mathbf{d}^e as follows:

$$\mathbf{q} = \mathbf{T} \mathbf{d} = \mathbf{T} \mathbf{N} \mathbf{d}^e \triangleq \mathbf{G} \mathbf{d}^e \tag{24}$$

According to all these definitions, Eq. (17) can be rewritten in its discretized form in the following way:

$$\begin{aligned} \sum_e \int_{-1}^1 \delta \mathbf{d}^{eT} \left(\int_{-h_k}^{h_k} (\mathbf{B}_L + \mathbf{B}_{NL}(\mathbf{d}))^T \mathcal{L} \left(\mathbf{B}_L + \frac{1}{2}\mathbf{B}_{NL}(\mathbf{d}) \right) dY \right) \mathbf{d}^e \frac{L_e}{2} d\xi \\ = \delta \mathbf{d}^T(0) \mathbf{T}^T \boldsymbol{\Phi}_0 + \delta \mathbf{d}^T(L) \mathbf{T}^T \boldsymbol{\Phi}_L \end{aligned} \tag{25}$$

where:

$$\begin{cases} \mathbf{B}_L = \mathbf{H} \mathbf{G} \\ \mathbf{B}_{NL} = \mathbf{A} \mathbf{G} \end{cases} \quad (k = s \text{ or } c) \tag{26}$$

and the integration over a real element is replaced by the integration over the reference element, by means of the fol-

lowing variable change: $dX = \frac{L_e}{2} d\xi$. A reduced numerical integration scheme (with 2 Gaussian points by element) is employed for the calculation of integrals in Eq. (25) so as to prevent from any shear-locking problem.

3.2 Derivation of the eigenproblem

The equilibrium equation (25) may be rewritten in the more concise following form:

$$\Psi(\mathbf{D}) = \mathbf{F} \quad (27)$$

where Ψ and \mathbf{F} designate the global internal and external force vectors, respectively, associated to the global nodal displacement vector \mathbf{D} .

Differentiating Eq. (27) allows one to compute the tangent stiffness matrix:

$$\mathbf{K}_T = \frac{\partial \Psi(\mathbf{D})}{\partial \mathbf{D}} \quad (28)$$

and to solve the bifurcation problem in hand by finding its eigenvalues and corresponding eigenvectors. This matrix is classically decomposed as follows:

$$\mathbf{K}_T = \mathbf{K}_0 + \mathbf{K}_{NL} + \mathbf{K}_\sigma \quad (29)$$

where \mathbf{K}_0 , \mathbf{K}_{NL} and \mathbf{K}_σ denote the small-strain, large-displacement and geometric stiffness matrices, respectively, whose expressions are given by:

$$\begin{cases} \mathbf{K}_0 = \sum_e \int_{-1}^1 \left(\int_{-h_k}^{h_k} \mathbf{B}_L^T \mathcal{L} \mathbf{B}_L dY \right) \frac{L_e}{2} d\xi \\ \mathbf{K}_{NL} = \sum_e \int_{-1}^1 \left(\int_{-h_k}^{h_k} \left(\mathbf{B}_L^T \mathcal{L} \mathbf{B}_{NL} + \mathbf{B}_{NL}^T \mathcal{L} \mathbf{B}_L + \mathbf{B}_{NL}^T \mathcal{L} \mathbf{B}_{NL} \right) dY \right) \frac{L_e}{2} d\xi \\ \mathbf{K}_\sigma d\mathbf{D} = \sum_e \int_{-1}^1 \left(\int_{-h_k}^{h_k} d\mathbf{B}_{NL}^T \mathbf{s} dY \right) \frac{L_e}{2} d\xi \end{cases} \quad (30)$$

In the case of small pre-buckling deformations, the non-linear eigenvalue problem comes down to the following linearized generalized eigenvalue problem:

$$(\mathbf{K}_0 + \lambda \mathbf{K}_\sigma) d\mathbf{D} = \mathbf{0} \quad (31)$$

where \mathbf{K}_σ is here the geometric stiffness matrix related to a unit reference load.

The critical loadings λ (eigenvalues) and the corresponding buckling modes $d\mathbf{D}$ (eigenvectors) are then determined

using the QZ algorithm implemented in standard Fortran sub-routines from the EISPACK package [25].

4 Results: validation, analysis and discussion

A home-made finite element program has been developed, based on the previous 1D enriched finite element model. Linearized buckling analyses are first performed in both cases of axial compression and pure bending of the sandwich beam-column. The numerical results are validated against the analytical solutions from Douville and Le Grogneq [23], recalled at the beginning of this paper (see Sect. 2.2).

For conciseness purposes, no parametric analysis will be addressed in the present paper. The interested reader may refer to Douville and Le Grogneq [23] for more details about the influence of geometric and material parameters on the buckling response of sandwich beam-columns.

The case of a cantilever sandwich beam with a concentrated transverse load at the free end is also investigated. Since there is no reference solution available in the literature for this loading case, the numerical results provided by the present 1D enriched model will be compared with the solutions obtained from full 2D computations performed using Abaqus software.

The same mesh is maintained throughout this study, displaying 100 elements along the length of the beam. A total number of 12 Gaussian points is retained for the numerical

integration through the core thickness, according to a preliminary convergence analysis.

4.1 Axial compression

The material and geometric parameters considered in this case are given in Table 1 (with two possible core thicknesses).

The displacement boundary conditions defined in Douville and Le Grogneq [23] and depicted in Fig. 2a are here appropriately applied at both ends of the column and no further loading is required. At the left end, the longitu-

Table 1 Material and geometric parameters in axial compression

E_s (MPa)	E_c (MPa)	ν_c	L (mm)	h_s (mm)	h_c (mm)
50000	70	0.4	600	0.5	15-30

dinal displacement of both core and skin layers is fixed, what corresponds to the following boundary conditions: $U^b(0) = U^a(0) = \theta^b(0) = \theta^a(0) = U_1^c(0) = \phi_3(0) = \phi_4(0) = U_0^c(0) = 0$. Conversely, at the right end, a uniform unit displacement is applied throughout the sandwich thickness in the longitudinal direction, in order to generate compressive stresses in the structure and induce a buckling phenomenon: $U^b(L) = U^a(L) = U_0^c(L) = -1$ and $\theta^b(L) = \theta^a(L) = U_1^c(L) = \phi_3(L) = \phi_4(L) = 0$. The transverse displacement of an arbitrary point is also fixed so as to prevent the column from rigid modes.

Based upon prior parametric analyses achieved for several geometric and material configurations, parameter α is definitively set to the following value:

$$\alpha = \frac{\pi}{20} \text{ mm}^{-1} \tag{32}$$

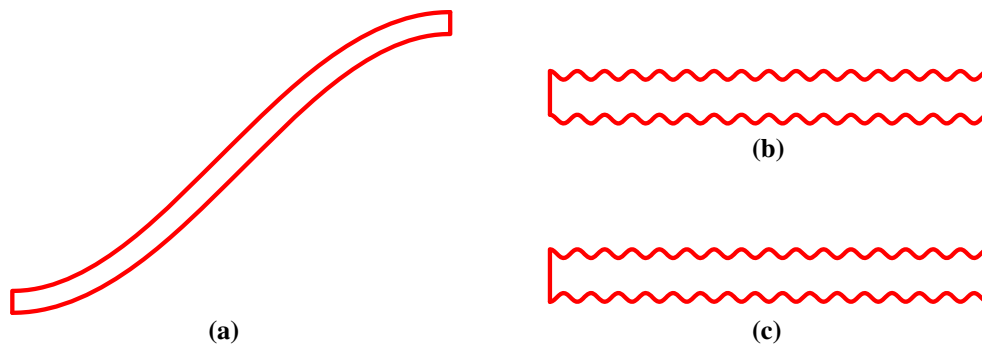


Fig. 4 2D reconstitution of global and local buckling modes obtained with the 1D model. **a** global mode, **b** antisymmetric local mode, **c** symmetric local mode

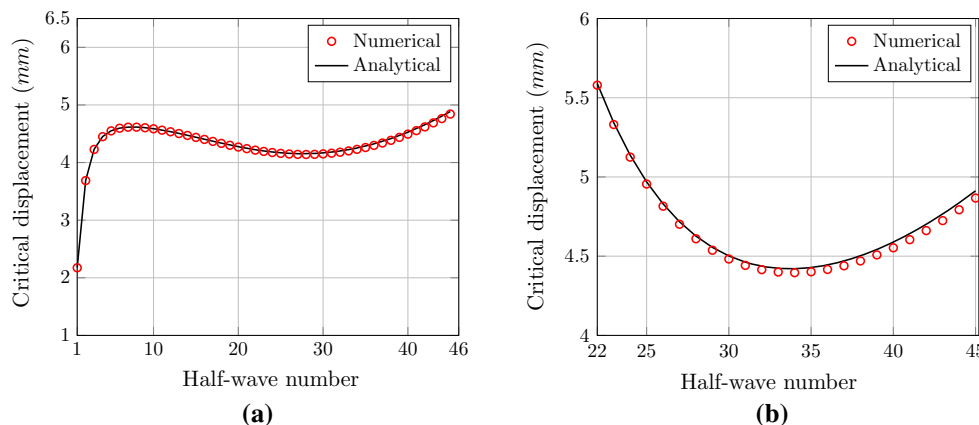


Fig. 5 Comparison between analytical and numerical (1D) critical displacements of a sandwich column with core thickness $h_c = 15$ mm. **a** antisymmetric modes, **b** symmetric modes

The 1D finite element model allows one to recover all the buckling mode types for sandwich columns under axial compression, which were identified in the previous analytical study. In particular, the first buckling mode is found to be a global mode when considering the lower core thickness ($h_c = 15$ mm) and either an antisymmetric or a symmetric local mode with the thicker core layer ($h_c = 30$ mm). Fig. 4 displays those three mode types, which were rebuilt from 1D simulation results.

In order to assess the accuracy of the 1D finite element model, the obtained antisymmetric and symmetric critical values are finally plotted versus the half-wave number, together with the analytical solutions provided by Eqs. (33) and (34). The comparison illustrated in Figs. 5 and 6 shows a fair agreement between the analytical and numerical results (with less than 1 % of relative error between the critical displacements).

4.2 Pure bending

In the pure bending case, the sandwich beam is characterized by the properties summarized in Table 2 with a varying core modulus E_c .

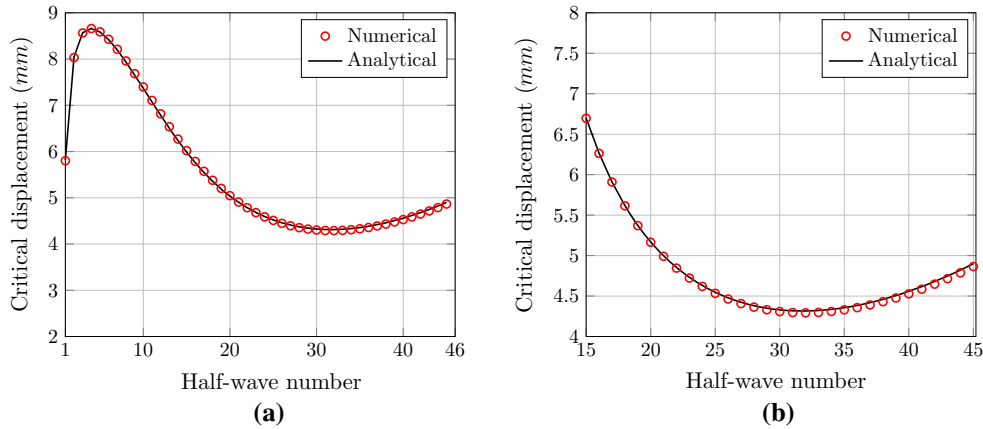


Fig. 6 Comparison between analytical and numerical (1D) critical displacements of a sandwich column with core thickness $h_c = 30$ mm. **a** antisymmetric modes, **b** symmetric modes

Table 2 Material and geometric parameters in pure bending

E_s (MPa)	E_c (MPa)	ν_c	L (mm)	h_s (mm)	h_c (mm)
65600	10-50-100	0.3	800	0.5	9

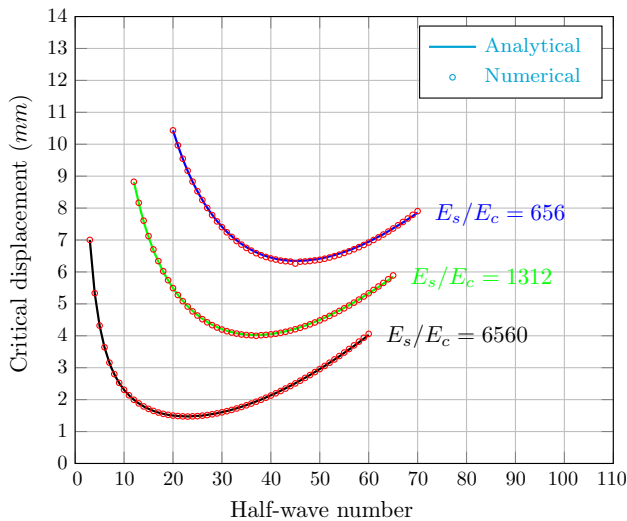


Fig. 7 Analytical and numerical critical displacements of a sandwich beam under pure bending

The boundary conditions are partially the same as in the preceding case, except for the right end of the sandwich beam, where uniform compressive and tensile displacements

are applied on the top and bottom skins, respectively. The new conditions can thus be expressed as follows: $U^b(0) = U^a(0) = \theta^b(0) = \theta^a(0) = U^c(0) = \phi_3(0) = \phi_4(0) = U^c_0(0) = \theta^b(L) = \theta^a(L) = 0$ and $U^b(L) = -U^a(L) = -1$.

Figure 7 depicts the analytical and numerical critical displacements corresponding to buckling modes with a large range of half-wave numbers, for the three considered core moduli. It reveals that the enriched numerical model is again in excellent agreement with the analytical solution. Both the critical values and buckling modes (half-wave numbers) are accurately estimated (the relative error does not exceed 1% in all cases).

The very first buckling mode (corresponding to the minimum critical displacement) of the sandwich beam with $E_c = 10$ MPa is shown in Fig. 8, displaying 23 half-waves. One can notice some deviations in the buckling mode shape from the expected regular sinusoidal pattern. Owing to the kinematics, the enforced displacements fatally lead here to a pre-critical stress state that does not comply accurately with the pure bending problem. In Douville and Le Grogneq [23], similar 2D numerical computations were performed with a linear distribution of displacements throughout the sandwich thickness, and the perfect analytical modes were thus captured. For verification purposes, a 2D numerical computation has been performed here using Abaqus software with the same imperfect boundary conditions, and the same modal deformed shape was obtained (see Fig. 8).

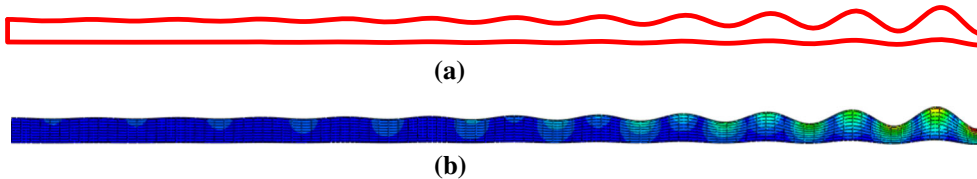


Fig. 8 Typical buckling mode of a sandwich beam under pure bending. **a** buckling mode obtained with the 1D model, **b** buckling mode obtained with Abaqus

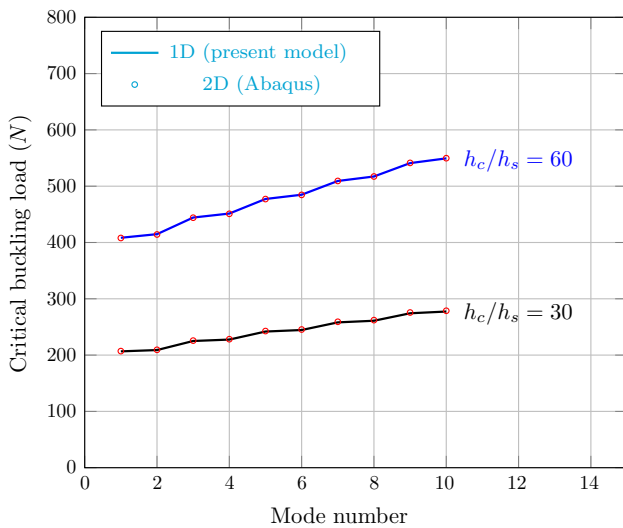


Fig. 9 Comparison between 1D and 2D numerical critical values of sandwich beams subjected to simple bending

4.3 Simple bending

One considers finally a sandwich beam under simple bending so as to demonstrate the wide range of applications of the present model. The left end of the sandwich beam is clamped whereas transverse concentrated forces are applied on the right end of the top and bottom faces (the core layer being load-free).

In the absence of analytical solutions, 2D finite element computations are performed here using Abaqus software, for validation purposes. The associated finite element mesh is made up of 8-node quadrangular elements with reduced integration. It displays 100 elements along the beam length, 8 elements in the thickness of the foam core and a unique element in the thickness of each skin.

The two different configurations whose geometric and material properties are listed in Table 1 are considered again (namely a relatively thin and thick beam, respectively). The results from the two numerical 1D and 2D approaches are

Table 3 Summary of the minimum critical values and related half-wave numbers

Loading	Case	λ_{cr}^{1D} / n	λ_{cr}^{ref} / n
Compression	$h_c = 15$ mm	2.174/1	2.178/1
	$h_c = 30$ mm	4.29/32	4.31/32
Pure bending	$E_c = 10$ MPa	1.474/23	1.47/23
	$E_c = 50$ MPa	4.027/37	4.03/37
	$E_c = 100$ MPa	6.349/45	6.35/45
Simple bending	$h_c = 15$ mm	206.62/-	207.09/-
	$h_c = 30$ mm	408.39/-	408.01/-

confronted for the first 10 buckling modes, and it can be clearly seen from Fig. 9 that the critical values are once more in very good accordance (with less than 0.5 % of relative error in the worst cases).

The typical buckling mode shape in this loading case is characterized by the appearance of wrinkles at the lower skin near the left end (where the axial compressive stresses are at their maximum). As depicted in Fig. 10, the 2D and rebuilt 1D buckling modes are also very similar (only the first mode of the thicker beam is displayed, for illustrative purposes).

Eventually, the critical values and related half-wave numbers obtained with the 1D present model are summed up in Table 3 together with the reference solutions (either analytical in the compression and pure bending cases or numerical in the simple bending case) for the very first buckling mode (the critical values are given in mm for the compression and pure bending cases and in N for the simple bending case).

It is worth mentioning that a unique value of parameter α has been retained throughout all the calculations, for which satisfactory results have been systematically obtained.

5 Conclusions

In this paper, an original beam-like model has been formulated and implemented for the purpose of investigating the

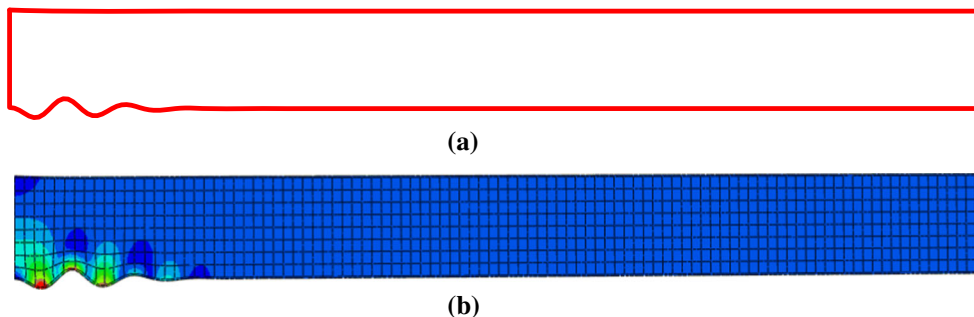


Fig. 10 Comparison of the 1D and 2D first buckling modes of the sandwich beam with $h_c/h_s = 60$ under simple bending. **a** buckling mode obtained with the 1D model, **b** buckling mode obtained with Abaqus

buckling behavior of sandwich beam-columns. In this model, the skins are classically represented by Timoshenko beams whereas special hyperbolic functions are employed so as to describe the displacement profiles along the core thickness. This kinematics is perfectly suited as it is based on previous analytical investigations where both global and local buckling modes are naturally described by the same hyperbolic functions (with variable half-wave numbers).

The problem is discretized using 3-node Lagrangian 1D elements with 14 degrees of freedom per node. The computation of the initial and geometric stiffness matrices is specially performed in order to solve the generalized eigenproblem encountered in linearized buckling analyses.

The numerical solutions provided by the present model are shown to be in very good agreement with reference analytical and numerical results, regardless of the loading conditions. This new 1D model appears thus to be a robust and computationally efficient tool for the general study of sandwich beam-columns in the presence of local effects. It has been successfully applied to buckling analyses and may be further employed in the context of post-buckling or vibration/dynamic problems.

Acknowledgments The authors are grateful to the Nord-Pas-de-Calais Regional Council (France) for its financial support.

Appendix A. Closed-form expressions for the critical displacements of a sandwich column

The critical displacements are given by the following expressions in the antisymmetric and symmetric cases, respectively:

$$\begin{aligned} \lambda_{cr}^A = & \left(4E_s E_c n \pi L^2 h_s \left[4n^2 \pi^2 h_s^2 + 3L^2 \right] \cosh^2 \frac{n\pi h_c}{L} \right. \\ & + \left[3E_c^2 L^5 + 12E_s E_c n^2 \pi^2 L^3 h_s^2 (1 - \nu_c) \right. \\ & + \left. 4E_s^2 n^4 \pi^4 L h_s^4 \left(3 + 2\nu_c - \nu_c^2 \right) \right] \\ & \left. \cosh \frac{n\pi h_c}{L} \sinh \frac{n\pi h_c}{L} \right. \\ & - 3E_c n \pi L^4 \left[4E_s h_s + E_c h_c \right] \\ & + 12E_s E_c n^3 \pi^3 L^2 h_s^2 h_c \left[1 + \nu_c \right] \\ & + \left. 4E_s^2 n^5 \pi^5 h_s^4 h_c \left[1 + \nu_c \right]^2 \right) / \\ & \left(12E_s n \pi L h_s \left[E_c L^2 \cosh^2 \frac{n\pi h_c}{L} \right. \right. \\ & + E_s n \pi h_s L \left(3 + 2\nu_c - \nu_c^2 \right) \cosh \frac{n\pi h_c}{L} \sinh \frac{n\pi h_c}{L} \\ & + \left. \left. E_s n^2 \pi^2 h_s h_c \left(1 + \nu_c \right)^2 \right] \right) \end{aligned} \quad (33)$$

$$\lambda_{cr}^S = \left(4E_s E_c n \pi L^2 h_s \left[4n^2 \pi^2 h_s^2 + 3L^2 \right] \cosh^2 \frac{n\pi h_c}{L} \right.$$

$$\begin{aligned} & + \left[3E_c^2 L^5 + 12E_s E_c n^2 \pi^2 L^3 h_s^2 (1 - \nu_c) \right. \\ & + \left. 4E_s^2 n^4 \pi^4 L h_s^4 \left(3 + 2\nu_c - \nu_c^2 \right) \right] \\ & \times \cosh \frac{n\pi h_c}{L} \sinh \frac{n\pi h_c}{L} \\ & + 3E_c^2 n \pi L^4 h_c \\ & - 16E_s E_c n^3 \pi^3 L^2 h_s^3 \\ & - 12E_s E_c n^3 \pi^3 L^2 h_s^2 h_c \left[1 + \nu_c \right] \\ & - \left. 4E_s^2 n^5 \pi^5 h_s^4 h_c \left[1 + \nu_c \right]^2 \right) / \\ & \left(12E_s n \pi L h_s \left[E_c L^2 \cosh^2 \frac{n\pi h_c}{L} \right. \right. \\ & + E_s n \pi h_s L \left(3 + 2\nu_c - \nu_c^2 \right) \cosh \frac{n\pi h_c}{L} \sinh \frac{n\pi h_c}{L} \\ & - \left. \left. E_c L^2 - E_s n^2 \pi^2 h_s h_c \left(1 + \nu_c \right)^2 \right] \right) \end{aligned} \quad (34)$$

Appendix B. Useful expressions in the core layer

The displacement gradient tensor components in the foam core write:

$$\begin{aligned} \mathcal{H}_{XX}^c &= U_{0,X}^c + U_{1,X}^c \sinh \left(\frac{\pi}{L} Y \right) + \phi_{1,X} \cosh(\alpha Y) \\ &+ \phi_{2,X} \sinh(\alpha Y) \\ &+ \phi_{3,X} Y \cosh(\alpha Y) + \phi_{4,X} Y \sinh(\alpha Y) \\ \mathcal{H}_{XY}^c &= U_1^c \frac{\pi}{L} \cosh \left(\frac{\pi}{L} Y \right) + \phi_{1\alpha} \sinh(\alpha Y) + \phi_{2\alpha} \cosh(\alpha Y) \\ &+ \phi_3 [\cosh(\alpha Y) + Y \alpha \sinh(\alpha Y)] \\ &+ \phi_4 [\sinh(\alpha Y) + Y \alpha \cosh(\alpha Y)] \\ \mathcal{H}_{YX}^c &= V_{0,X}^c \cosh \left(\frac{\pi}{L} Y \right) + V_{1,X}^c Y + \phi_{5,X} \cosh(\alpha Y) \\ &+ \phi_{6,X} \sinh(\alpha Y) + \phi_{7,X} Y \cosh(\alpha Y) \\ &+ \phi_{8,X} Y \sinh(\alpha Y) \\ \mathcal{H}_{YY}^c &= V_0^c \frac{\pi}{L} \sinh \left(\frac{\pi}{L} Y \right) + V_1^c + \phi_5 \alpha \sinh(\alpha Y) \\ &+ \phi_6 \alpha \cosh(\alpha Y) + \phi_7 [\cosh(\alpha Y) + Y \alpha \sinh(\alpha Y)] \\ &+ \phi_8 [\sinh(\alpha Y) + Y \alpha \cosh(\alpha Y)] \end{aligned} \quad (35)$$

Taking into account the displacement continuity constraints at the interfaces, $\phi_{1,X}$, $\phi_{2,X}$, $\phi_{5,X}$ and $\phi_{6,X}$ can be given by the following expressions:

$$\begin{aligned} \phi_{1,X} &= \frac{1}{\cosh(\alpha h_c)} \left(\frac{1}{2} (U_{,X}^b + U_{,X}^a) + \frac{h_s}{2} (\theta_{,X}^b - \theta_{,X}^a) \right. \\ & \left. - U_{0,X}^c - \phi_{4,X} h_c \sinh(\alpha h_c) \right) \\ \phi_{2,X} &= \frac{1}{\sinh(\alpha h_c)} \left(\frac{1}{2} (U_{,X}^b - U_{,X}^a) + \frac{h_s}{2} (\theta_{,X}^b + \theta_{,X}^a) \right. \\ & \left. - U_{1,X}^c \sinh \left(\frac{\pi}{L} h_c \right) - \phi_{3,X} h_c \cosh(\alpha h_c) \right) \end{aligned}$$

$$\begin{aligned} \phi_{5,x} &= \frac{1}{\cosh(\alpha h_c)} \left(\frac{1}{2}(V_{,x}^b + V_{,x}^a) - V_{0,x}^c \cosh\left(\frac{\pi}{L} h_c\right) \right. \\ &\quad \left. - \phi_{8,x} h_c \sinh(\alpha h_c) \right) \\ \phi_{6,x} &= \frac{1}{\sinh(\alpha h_c)} \left(\frac{1}{2}(V_{,x}^b - V_{,x}^a) - V_{1,x}^c h_c \right. \\ &\quad \left. - \phi_{7,x} h_c \cosh(\alpha h_c) \right) \end{aligned} \tag{36}$$

Appendix C. Useful matrices

The non-zero components of matrix **H** are:

$$\begin{aligned} H(1, 4) &= 1 & H(1, 12) &= -Y \\ H(2, 8) &= 1 & H(2, 10) &= -1 \\ H(3, 3) &= \frac{\cosh(\alpha Y)}{2 \cosh(\alpha h_c)} + \frac{\sinh(\alpha Y)}{2 \sinh(\alpha h_c)} \\ H(3, 4) &= \frac{\cosh(\alpha Y)}{2 \cosh(\alpha h_c)} - \frac{\sinh(\alpha Y)}{2 \sinh(\alpha h_c)} \\ H(3, 11) &= \frac{h_s \cosh(\alpha Y)}{2 \cosh(\alpha h_c)} + \frac{h_s \sinh(\alpha Y)}{2 \sinh(\alpha h_c)} \\ H(3, 12) &= \frac{h_s \sinh(\alpha Y)}{2 \sinh(\alpha h_c)} - \frac{h_s \cosh(\alpha Y)}{2 \cosh(\alpha h_c)} \\ H(3, 14) &= \sinh\left(\frac{\pi}{L} Y\right) - \frac{\sinh(\alpha Y) \sinh\left(\frac{\pi}{L} h_c\right)}{\sinh(\alpha h_c)} \\ H(3, 21) &= Y \cosh(\alpha Y) - \frac{h_c \sinh(\alpha Y)}{\tanh(\alpha h_c)} \\ H(3, 22) &= Y \sinh(\alpha Y) - h_c \tanh(\alpha h_c) \cosh(\alpha Y) \\ H(3, 26) &= 1 - \frac{\cosh(\alpha Y)}{\cosh(\alpha h_c)} \\ H(4, 5) &= \frac{\alpha \sinh(\alpha Y)}{2 \cosh(\alpha h_c)} + \frac{\alpha \cosh(\alpha Y)}{2 \sinh(\alpha h_c)} \\ H(4, 6) &= \frac{\alpha \sinh(\alpha Y)}{2 \cosh(\alpha h_c)} - \frac{\alpha \cosh(\alpha Y)}{2 \sinh(\alpha h_c)} \\ H(4, 15) &= \frac{\pi}{L} \sinh\left(\frac{\pi}{L} Y\right) - \frac{\alpha \sinh(\alpha Y) \cosh\left(\frac{\pi}{L} h_c\right)}{\cosh(\alpha h_c)} \\ H(4, 19) &= \cosh(\alpha Y) + Y \alpha \sinh(\alpha Y) - \frac{h_c \alpha \cosh(\alpha Y)}{\tanh(\alpha h_c)} \\ H(4, 20) &= \sinh(\alpha Y) + Y \alpha \cosh(\alpha Y) \\ &\quad - h_c \tanh(\alpha h_c) \alpha \sinh(\alpha Y) \\ H(4, 27) &= 1 - \frac{h_c \alpha \cosh(\alpha Y)}{\sinh(\alpha h_c)} \\ H(5, 1) &= \frac{\alpha \sinh(\alpha Y)}{2 \cosh(\alpha h_c)} + \frac{\alpha \cosh(\alpha Y)}{2 \sinh(\alpha h_c)} \\ H(5, 2) &= \frac{\alpha \sinh(\alpha Y)}{2 \cosh(\alpha h_c)} - \frac{\alpha \cosh(\alpha Y)}{2 \sinh(\alpha h_c)} \end{aligned}$$

$$\begin{aligned} H(5, 7) &= \frac{\sinh(\alpha Y)}{2 \sinh(\alpha h_c)} + \frac{\cosh(\alpha Y)}{2 \cosh(\alpha h_c)} \\ H(5, 8) &= \frac{\cosh(\alpha Y)}{2 \cosh(\alpha h_c)} - \frac{\sinh(\alpha Y)}{2 \sinh(\alpha h_c)} \\ H(5, 9) &= \frac{h_s \alpha \sinh(\alpha Y)}{2 \cosh(\alpha h_c)} + \frac{h_s \alpha \cosh(\alpha Y)}{2 \sinh(\alpha h_c)} \\ H(5, 10) &= \frac{h_s \alpha \cosh(\alpha Y)}{2 \sinh(\alpha h_c)} - \frac{h_s \alpha \sinh(\alpha Y)}{2 \cosh(\alpha h_c)} \\ H(5, 13) &= \frac{\pi}{L} \cosh\left(\frac{\pi}{L} Y\right) - \frac{\alpha \sinh\left(\frac{\pi}{L} h_c\right) \cosh(\alpha Y)}{\sinh(\alpha h_c)} \\ H(5, 16) &= \cosh\left(\frac{\pi}{L} Y\right) - \frac{\cosh\left(\frac{\pi}{L} h_c\right) \cosh(\alpha Y)}{\cosh(\alpha h_c)} \\ H(5, 17) &= \cosh(\alpha Y) + Y \alpha \sinh(\alpha Y) - \frac{h_c \alpha \cosh(\alpha Y)}{\tanh(\alpha h_c)} \\ H(5, 18) &= \sinh(\alpha Y) + Y \alpha \cosh(\alpha Y) \\ &\quad - h_c \alpha \tanh(\alpha h_c) \sinh(\alpha Y) \\ H(5, 23) &= Y \cosh(\alpha Y) - \frac{h_c \sinh(\alpha Y)}{\tanh(\alpha h_c)} \\ H(5, 24) &= Y \sinh(\alpha Y) - h_c \tanh(\alpha h_c) \cosh(\alpha Y) \\ H(5, 25) &= -\frac{\sinh(\alpha Y)}{\cosh(\alpha h_c)} \\ H(5, 28) &= Y - \frac{h_c \sinh(\alpha Y)}{\sinh(\alpha h_c)} \\ H(6, 3) &= 1 & H(6, 11) &= -Y \\ H(7, 7) &= 1 & H(7, 9) &= -1 \end{aligned} \tag{37}$$

The constitutive matrix **L** is defined by the following non-zero components:

$$\begin{aligned} \mathcal{L}(1, 1) &= E_s, & \mathcal{L}(2, 2) &= \mu_s, & \mathcal{L}(3, 3) &= \Lambda_c^* + 2\mu_c \\ \mathcal{L}(3, 4) &= \mathcal{L}(4, 3) = \Lambda_c^*, & \mathcal{L}(4, 4) &= \Lambda_c^* + 2\mu_c, \\ \mathcal{L}(5, 5) &= \mu_c, & \mathcal{L}(6, 6) &= E_s, & \mathcal{L}(7, 7) &= \mu_s \end{aligned} \tag{38}$$

References

1. Timoshenko SP (1921) On the correction for shear of the differential equation for transverse vibrations of prismatic bars. Lond Edinb Dublin Philos Mag J Sci 41:744–746
2. Reissner E (1945) The effect of transverse shear deformation on the bending of elastic plates. J Appl Mech 12:69–77
3. Dong SB, Alpdogan C, Taciroglu E (2010) Much ado about shear correction factors in Timoshenko beam theory. Int J Solids Struct 47(13):1651–1665
4. Ambartsumian SA (1958) On the theory of bending plates. Izv Otd Tech Nauk AN SSSR 5:69–77
5. Reddy JN (1984) A refined non-linear theory of plates with transverse shear deformation. Int J Solids Struct 9–10(20):881–896
6. Touratier M (1991) An efficient standard plate theory. Int J Eng Sci 29(8):901–916

7. Soldatos KP (1992) A transverse shear deformation theory for homogeneous monoclinic plates. *Acta Mech* 94:195–220
8. Sayyad AS (2013) Flexure of thick orthotropic plates by exponential shear deformation theory. *Latin Am J Solids Struct* 10(3):473–490
9. Demasi L (2009) ∞^6 Mixed plate theories based on the generalized unified formulation. Part II: Layerwise theories. *Compos Struct* 87(1):12–22
10. Liu D, Li X (1996) An overall view of laminate theories based on displacement hypothesis. *J Compos Mater* 30(14):1539–1561
11. Reddy JN (1993) An evaluation of equivalent-single-layer and layerwise theories of composite laminates. *Compos Struct* 1–4(25):21–35
12. Carrera E (2002) Theories and finite elements for multilayered, anisotropic, composite plates and shells. *Arch Comput Methods Eng* 9(2):87–140
13. Reddy JN, Robbins DH (1994) Theories and computational models for composite laminates. *Appl Mech Rev* 47(6):147–169
14. Toledano A, Murakami H (1987) A composite plate theory for arbitrary laminate configurations. *J Appl Mech* 54(1):181–189
15. Di Sciuva M (1984) A refined transverse shear deformation theory for multilayered anisotropic plates. *Atti Della Accad Delle Sci Di Torino* 118:279–295
16. Tessler A, Di Sciuva M, Gherlone M (2010) A consistent refinement of first-order shear deformation theory for laminated composite and sandwich plates using improved zigzag kinematics. *J Mech Mater Struct* 5(2):341–367
17. Carrera E (2003) Theories and finite elements for multilayered plates and shells: a unified compact formulation with numerical assessment and benchmarking. *Arch Comput Methods Eng* 10(3):215–296
18. Ghugal YM, Shimpi RP (2002) A review of refined shear deformation theories of isotropic and anisotropic laminated plates. *J Reinf Plastics Compos* 21(9):775–813
19. Zhen W, Wanji C (2008) An assessment of several displacement-based theories for the vibration and stability analysis of laminated composite and sandwich beams. *Compos Struct* 84(4):337–349
20. Hu H, Belouettar S, Potier-Ferry M, Daya EM (2008) Review and assessment of various theories for modeling sandwich composites. *Compos Struct* 84(3):282–292
21. Phan CN, Bailey NW, Kardomateas GA, Battley MA (2012) Wrinkling of sandwich wide panels/beams based on the extended high-order sandwich panel theory: formulation, comparison with elasticity and experiments. *Arch Appl Mech* 10–11:1585–1599
22. Hu H, Belouettar S, Potier-Ferry M, Makrati A (2009) A novel finite element for global and local buckling analysis of sandwich beams. *Compos Struct* 90(3):270–278
23. Douville MA, Le Grogne P (2013) Exact analytical solutions for the local and global buckling of sandwich beam-columns under various loadings. *Int J Solids Struct* 16–17:2597–2609
24. Sad Saoud K, Le Grogne P (2014) A unified formulation for the biaxial local and global buckling analysis of sandwich panels. *Thin-Walled Struct* 82:13–23
25. Smith BT, Boyle JM, Dongarra JJ, Garbow BS, Ikebe Y, Klema VC, Moler CB (1976) *Matrix eigensystem routines-EISPACK guide lecture notes in computer science*, vol 6. Springer, New York